NATURE|Vol 453|19 June 2008|doi:10.1038/nature07125

# Entangled states of trapped atomic ions

Rainer Blatt[1,2] & David Wineland[3]

**To process information using quantum-mechanical principles, the states of individual particles need to be entangled and manipulated. One way to do this is to use trapped, laser-cooled atomic ions. Attaining a general-purpose quantum computer is, however, a distant goal, but recent experiments show that just a few entangled trapped ions can be used to improve the precision of measurements. If the entanglement in such systems can be scaled up to larger numbers of ions, simulations that are intractable on a classical computer might become possible.**

For more than five decades, quantum superposition states that are coherent have been studied and used in applications such as photon interferometry and Ramsey spectroscopy[1]. However, entangled states, particularly those that have been 'engineered' or created for specific tasks, have become routinely available only in the past two decades (see page 1004). The initial experiments with pairs of entangled photons[2,3], starting in the 1970s, were important because they provided tests of non-locality in quantum mechanics[4]. Then, in the early to mid-1980s, Richard Feynman and David Deutsch proposed that it might be possible way to carry out certain computations or quantum simulations efficiently by using quantum systems[5,6]. This idea was, however, largely considered a curiosity until the mid-1990s, when Peter Shor devised an algorithm[7] that could factor large numbers very efficiently with a quantum computer. This marked the beginning of widespread interest in quantum information processing[8] and stimulated several proposals for the implementation of a quantum computer.

Among these proposals, the use of trapped ions[9] has proved to be one of the most successful ways of deterministically creating entangled states, and for manipulating, characterizing and using these states for measurement. At present, about 25 laboratories worldwide are studying aspects of quantum information processing with trapped ions. Ions provide a relatively 'clean' system, because they can be confined for long durations while experiencing only small perturbations from the environment, and can be coherently manipulated. Although trapping ions in this way involves several technical processes, the system is an accessible one in which to test concepts that might be applicable to other systems, such as those involving neutral trapped atoms, quantum dots, nuclear spins, Josephson junctions or photons.

In this review, we highlight recent progress in creating and manipulating entangled states of ions, and we describe how these advances could help to generate quantum gates for quantum information processing and improve tools for high-precision measurement. For a review of earlier progress in quantum information processing with atoms, including atomic ions, and photons, see ref. 10.

## Trapped and laser-cooled ions

To study entanglement, it is desirable to have a collection of quantum systems that can be individually manipulated, their states entangled, and their coherences maintained for long durations, while suppressing the detrimental effects of unwanted couplings to the environment. This can be realized by confining and laser cooling a group of atomic ions in a particular arrangement of electric and/or magnetic fields[11,12]. With such 'traps', atomic ions can be stored nearly indefinitely and can be localized in space to within a few nanometres. Coherence times of as long as ten minutes have been observed for superpositions of two hyperfine atomic states of laser-cooled, trapped atomic ions[13,14].

In the context of quantum information processing, a typical experiment involves trapping a few ions by using a combination of static and sinusoidally oscillating electric potentials that are applied between the electrodes of a linear quadrupole, an arrangement known as a Paul trap[12] (Fig. 1). When the trapped ions are laser cooled, they form a linear 'string', in which the spacings are determined by a balance between the horizontal (axial) confining fields and mutual Coulomb repulsion. Scattered fluorescence, induced by a laser beam, can be imaged with a camera (Fig. 1). The use of tightly focused laser beams allows the manipulation of individual ions.

For simplicity, in this review, we focus on two specific internal states of each ion, which we refer to as the ground and excited states ($|g\rangle$ and $|e\rangle$, respectively). This 'quantum bit' (qubit) structure is 'dressed' by the oscillator states $|n\rangle$ of frequency $\omega_{\mathrm{m}}$ of a particular mode (Fig. 1). We denote the internal states as 'spin' states, in analogy to the two states of a spin −½ particle. If the energy between internal states corresponds to an optical frequency $\omega_{eg}$, this atomic transition can be driven by laser radiation at frequency $\omega_{eg}$, which couples states $|g, n\rangle \leftrightarrow |e, n\rangle$, where $|g, n\rangle$ denotes the combined state $|g\rangle|n\rangle$. Spin and motional degrees of freedom can be coupled by tuning the laser to 'sideband' frequencies $\omega_{eg} \pm \omega_{\mathrm{m}}$, which drives transitions $|g, n\rangle \leftrightarrow |e, n+\Delta n\rangle$ (refs 15–18), with $\Delta n = \pm 1$. In this case, state evolution can be described as a rotation $R_{\Delta n}(\theta, \phi)$ of the state vector on the Bloch sphere[8,18] and is defined here as

$$R_{\Delta n}(\theta, \phi)\,|g, n\rangle \rightarrow \cos\frac{\theta}{2}|g, n\rangle + ie^{i\phi}\sin\frac{\theta}{2}|e, n+\Delta n\rangle$$

$$R_{\Delta n}(\theta, \phi)\,|e, n+\Delta n\rangle \rightarrow ie^{-i\phi}\sin\frac{\theta}{2}|g, n\rangle + \cos\frac{\theta}{2}|e, n+\Delta n\rangle \quad (1)$$

where $\theta$ depends on the strength and the duration of the applied laser pulse, $\phi$ is the laser beam phase at the ion's position and $i = \sqrt{-1}$. For $\Delta n = \pm 1$, entanglement is generated between the spin and motional degrees of freedom. Higher-order couplings ($|\Delta n| > 1$) are suppressed for laser-cooled ions, the spatial extent of which is much smaller than the laser wavelength, which is known as the Lamb–Dicke regime. In this regime, sideband laser cooling works by tuning the laser to induce absorption on the lower sideband frequency ($\Delta n = -1$), followed by spontaneous emission decay, which occurs mainly at the 'carrier'

[1]Institut für Experimentalphysik, Universität Innsbruck, Technikerstrasse 25, A-6020 Innsbruck, Austria. [2]Institut für Quantenoptik und Quanteninformation, Österreichische Akademie der Wissenschaften, Otto-Hittmair-Platz 1, A-6020 Innsbruck, Austria. [3]National Institute of Standards and Technology, 325 Broadway, Boulder, Colorado 80305, USA.

transition frequency ($\Delta n = 0$). With repeated absorption–emission cycles, the ions are optically pumped to the combined spin and motion ground state $|g, n=0\rangle$ (ref. 19). If the spin energy levels correspond to microwave or lower frequencies (as occurs in hyperfine atomic states and Zeeman states), the same processes can be realized by replacing single-photon optical transitions with two-photon stimulated-Raman transitions and by replacing spontaneous emission with spontaneous Raman scattering[15–18]. It should be noted that there are similarities between the coupling of an ion's internal states to the harmonic oscillator associated with a mode of motion and the case of cavity quantum electrodynamics, in which an atom's internal states are coupled to the harmonic oscillator associated with a single electromagnetic mode of the cavity (see page 1023).

The qubit state of an ion can be detected with more than 99% efficiency by measuring resonance fluorescence from an auxiliary state that is strongly coupled (by a monitoring excitation) to one of the qubit states ($|g\rangle$ or $|e\rangle$) and decays back only to that same state, known as a cycling transition. This is usually called quantum non-demolition (QND) detection because when the ion has been projected into a particular spin state, it will remain in that state throughout repeated excitation–emission cycles. Therefore, a cycle can be repeated many times, and it is not necessary to detect every emitted photon to obtain a high overall detection efficiency. If the qubit is projected to, or 'shelved' in, the state that is not coupled to the fluorescing transition, then no photons are observed, and this state can therefore be distinguished from the fluorescing state[20].

## Spin-entangled states

In 1995, Ignacio Cirac and Peter Zoller suggested how to use a trapped-ion system to implement a quantum computer[9]. For universal quantum computing and for the generation of arbitrary entangled qubit states, two basic gate operations are required: first, individual qubit rotations as described by equation (1); and, second, a two-qubit-entangling operation that is the quantum counterpart to the classical operation with the XOR logic gate, the controlled-NOT (CNOT)-gate operation. The CNOT gate flips the state of a target qubit depending on the state of a control qubit. And, importantly, when applied to superposition states, it generates entanglement. The CNOT operation (Fig. 2) is achieved with a sequence of carrier pulses ($R_0(\theta, \phi)$) and red sideband pulses ($R_{-1}(\theta, \phi)$). The central part of this sequence involves a 'phase gate' that applies a phase shift $e^{i\pi} = -1$ to the $|g, n=1\rangle$ component of the target ion's wavefunction. This is implemented by applying a coherent $R_{-1}(2\pi, \phi)$ pulse between the $|g, 1\rangle$ state and an auxiliary state $|\text{aux}, 0\rangle$. Because the applied radiation cannot excite the states $|g, 0\rangle$, $|e, 0\rangle$ or $|e, 1\rangle$, they are unaffected. This operation is sandwiched between rotations that transfer phase changes into state changes, as occurs in Ramsey spectroscopy. By using a single ion, Christopher Monroe *et al.*[21] realized the CNOT operation between motion and spin for $^9Be^+$ ions. Subsequently, Ferdinand Schmidt-Kaler *et al.*[22,23] and later Mark Riebe *et al.*[24] realized the complete CNOT operation between two individually addressed $^{40}Ca^+$ ions. Entangling gates have also been realized by irradiating ions simultaneously (Fig. 3). Although such gates can be implemented in a single step, they still involve transitory entanglement with a motional mode, which effectively couples the spin qubits. Ions have also been entangled with each other in a probabilistic way mediated by entanglement with scattered photons[25] (Fig. 4).

By sequentially combining single-qubit and multiqubit operations, various entangled states of ions have been created deterministically or 'on demand'. A research group from the National Institute of Standards and Technology (NIST), in Boulder, Colorado, created[26] the state $|\Psi_e(\phi)\rangle = \frac{3}{5}|ge\rangle - e^{i\phi}\frac{4}{5}|eg\rangle$, where $\phi$ is a controllable phase factor and $|ge\rangle$ denotes the combined state $|g\rangle_1|e\rangle_2$ for ions 1 and 2. More generally, by using entangling operations and single-qubit rotations with adjustable phases, all Bell states — $|\Psi^{\pm}\rangle = \frac{1}{\sqrt{2}}(|ge\rangle \pm |eg\rangle)$, $|\Phi^{\pm}\rangle = \frac{1}{\sqrt{2}}(|gg\rangle \pm |ee\rangle)$ — and arbitrary superpositions can be generated[27,28]. The quality or fidelity of quantum states is usually characterized by the degree with which they agree with the desired (or ideal) state, which is expressed as

$$F = \langle \Psi_{\text{ideal}} | \rho_{\text{exp}} | \Psi_{\text{ideal}} \rangle \qquad (2)$$

where $\rho_{\text{exp}}$ is the experimentally achieved density matrix, which characterizes both pure and non-pure states. In current experiments, fidelities $F > 0.95$ are achieved.

In some cases, complete knowledge of the density matrix is not required. For example, the fidelity of a state relative to $|\Phi^+\rangle$ can be derived from just three matrix elements, $F = \frac{1}{2}(\rho_{gg,gg} + \rho_{ee,ee}) + \text{Re}\rho_{ee,gg}$, where $\rho_{ee,gg} \equiv \langle ee|\rho_{\text{exp}}|gg\rangle$ and so on and Re denotes the real part of the expression that follows. The matrix elements $\rho_{gg,gg}$ and $\rho_{ee,ee}$ are obtained from the measured populations of the respective states. The matrix element $\rho_{ee,gg}$

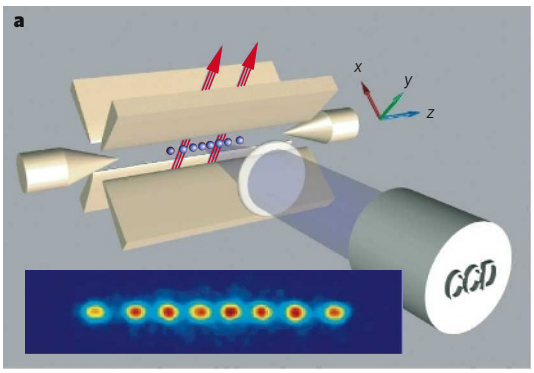


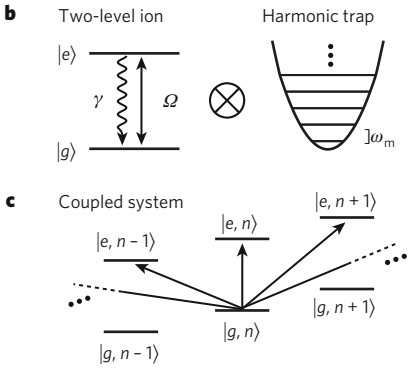


**Figure 1 | Ions confined in a trap. a**, A linear quadrupole ion trap (known as a Paul trap; beige) containing individually addressed $^{40}Ca^+$ ions (blue) is depicted. After cooling by laser beams (red), the trapped ions form a string and are then imaged by using a charge-coupled device (CCD). In the CCD image shown, the spacing of the two centre ions is ~8 μm. The electrode arrangement in the Paul trap provides an almost harmonic three-dimensional well. For a single ion, this is characterized by three frequencies[17]: $\omega_x$, $\omega_y$ and $\omega_z$, where $x$, $y$ and $z$ denote the confining potential axes. In this case, $z$ points along the trap axis and $x$, $y$ in the transverse directions. Owing to the Coulomb coupling that occurs between ions, the motion is best described in terms of normal modes; a string of ions can therefore be viewed as a pseudo-molecule. In general, the normal-mode frequencies $\omega_m$ differ from each other, and a particular mode can be accessed by spectral selection. **b**, The energy levels of a two-level ion (left) and one mode of the ion's motion (right) are shown. On the left is depicted the ion's ground state $|g\rangle$ and excited state $|e\rangle$, interacting with radiation characterized by the Rabi frequency $\Omega$ and decaying with the rate $\gamma$. On the right is depicted the harmonic oscillator potential and equally spaced energy levels for one mode of motion. Both the two-level system and the harmonic oscillator can be described jointly in a quantum-mechanical way, indicated by the direct product $\otimes$, resulting in a manifold of two-level systems separated by the mode frequency $\omega_m$ (as shown in **c**). **c**, The level structure of the coupled ion–harmonic-oscillator system is shown, with states jointly described by the spin ($|g\rangle$ and $|e\rangle$) and motional ($|0\rangle, |1\rangle, \ldots, |n\rangle$) degrees of freedom, where $|g\rangle|n\rangle = |g, n\rangle$ and $|e\rangle|n\rangle = |e, n\rangle$. Arrows indicate the transitions that are possible when appropriately tuned radiation is applied; dashed lines indicated connections to levels not shown.

can be obtained by applying a rotation $R_0(\pi/2, \phi)$ to both ions and measuring the parity $P \equiv |gg\rangle\langle gg| + |ee\rangle\langle ee| - |ge\rangle\langle ge| - |eg\rangle\langle eg|$ of the resultant state as a function of $\phi$. The only component of the parity that oscillates sinusoidally with frequency $2\phi$ is proportional to $\rho_{ee,gg}$, which allows this element to be extracted[29].

As shown by equation (2), the fidelity can be obtained by measuring the full density matrix. To do this, the quantum state in question must be prepared many times; in this way, with the appropriate single-qubit rotations applied before the qubit measurements, all expectation values of the density matrix are obtained. Such a procedure is known as quantum-state tomography[28]. When this procedure is applied to Bell states, the density matrix can be completely characterized (Fig. 5). From the density matrices, all measures can subsequently be calculated. For example, in the case of Bell's inequalities, it is possible to determine the expectation value of the operator[30] $A = \sigma_x^{(1)} \otimes \sigma_{x-z}^{(2)} + \sigma_x^{(1)} \otimes \sigma_{x+z}^{(2)} + \sigma_z^{(1)} \otimes \sigma_{x-z}^{(2)} - \sigma_z^{(1)} \otimes \sigma_{x+z}^{(2)}$, where $\sigma_{x\pm z} = (\sigma_x \pm \sigma_z)/\sqrt{2}$ and $\sigma$ is a Pauli operator and the superscripts refer to the first and second qubits. For local realistic theories, measurements of $|\langle A \rangle|$ are predicted to be less than 2, and values of $2 < |\langle A \rangle| < 2\sqrt{2}$ are expected for states that can be described only by quantum theory. With trapped ions, experiments yielded $|\langle A \rangle| = 2.25(3)$ at NIST[27], $|\langle A \rangle| = 2.52(6)$ at the Institute for Experimental Physics, University of Innsbruck (Innsbruck, Austria)[28], and $|\langle A \rangle| = 2.20(3)$ at the FOCUS Center and Department of Physics, University of Michigan (Ann Arbor, Michigan)[31], where the number in parentheses denotes the uncertainty in the last digit, clearly corroborating quantum theory (Fig. 5). Moreover, each time an experiment was run, a result was recorded. This closed the 'detection loophole', which would provide a way to violate Bell's inequalities within local realistic theories.

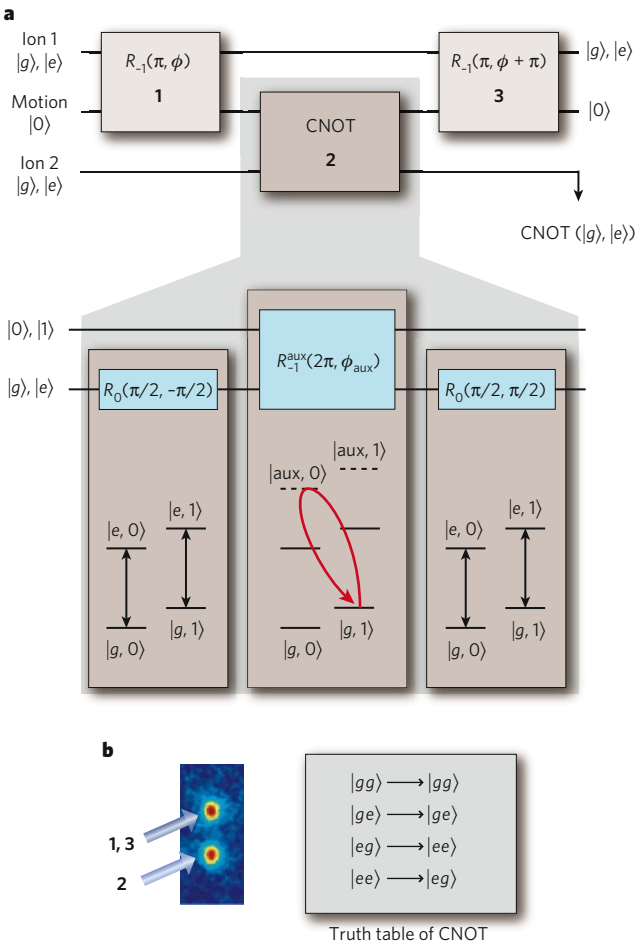


**Figure 2 | A CNOT-gate operation with two trapped ions. a**, Consider two ions in the same trap that are initially prepared in their motional ground state. In step 1, a lower-sideband pulse $R_{-1}(\pi, \phi)$ is applied to the first ion (ion 1; the control qubit) and maps the excited-state amplitude of this ion to the first excited state of a selected motional mode (a process known as a SWAP operation). Importantly, this motional excitation is also shared with the second ion (ion 2; the target qubit). In step 2, a CNOT-gate operation is implemented between the motion qubit (which is shared by both spin qubits) and the spin state of ion 2. Finally, in step 3, the first step is reversed, thereby restoring the initial spin state of ion 1 and returning the motion to its ground state. The pulse sequence of the CNOT-gate operation is also shown (lower part of **a**). **b**, On the left is a CCD image of two ions. The arrows indicate laser radiation that is applied to the ions in the order of the indicated numbers (which correspond to the three steps in **a**). First, a laser pulse is applied to the upper ion (1), then the CNOT sequence is applied to the lower ion (2). Finally, a laser pulse is applied to the upper ion again (3). On the right is the resultant truth table of the CNOT-gate operation, with the first and second symbols denoting the state of the control qubit (ion 1) and the target qubit (ion 2), respectively.

With trapped ions, cat states with $|\alpha| = |\beta|$ have been generated by using two approaches. At NIST, global entangling operations were used to demonstrate a cat state of four ions[29], a GHZ state with $F = 0.89$ (ref. 37), and cat states of up to six ions[38]. Using individually addressed ions and a CNOT-gate operation, the research group at Innsbruck produced GHZ states in an algorithmic way and analysed the states by using tomographic measurements[39]. In a similar way, the Innsbruck group also produced W states for $N$-ion qubits, $|\Psi_W\rangle = \frac{1}{\sqrt{N}}(|g \ldots gge\rangle + |g \ldots geg\rangle + \ldots + |eg \ldots g\rangle)$, which belong to a different class of entangled states. Such classes are distinct because states of different classes cannot be transformed into each other by local operations and classical communication[40]. Nevertheless, both cat and W states can violate Bell-type inequalities. In contrast to cat states, W states are remarkably robust in the face of a variety of decoherence processes: for W states, even the loss of qubits does not destroy entanglement completely. The Innsbruck group deterministically prepared an eight-qubit W state[41] by using individual ion addressing. Both the NIST and Innsbruck groups verified multipartite entanglement by using an 'entanglement witness', an operator constructed so that its expectation value must exceed (or be less than) a certain value to verify $N$-particle entanglement[38,41].

## Demonstrating quantum-information-processing algorithms

Algorithms are lists of instructions for completing a task[8]. As is the case in classical computation, quantum algorithms can sometimes be viewed as subroutines in a larger computation. A quantum-information-processing algorithm generally involves single-qubit gates and multiqubit gates, as well as measurements and measurement-dependent operations. The result of such a sequence of operations could be a deterministically prepared quantum state (such as a Bell, GHZ or W state), a conditioned state (such as an error-corrected state) or a state that is subsequently inferred from a measurement of the quantum register and is then available as classical information.

In contrast to classical information processing, quantum information processing allows tests to be carried out using superpositions. A simple example showing the gain in efficiency that is possible with a quantum algorithm was proposed by Deutsch and Richard Jozsa[42]. The Deutsch–Jozsa algorithm was first demonstrated with two qubits in nuclear magnetic resonance spectroscopy[43], and it was demonstrated more recently with a trapped ion[44], with the motional and spin properties of the ion qubit serving as the two qubits.

Another example algorithm is teleportation of the state of one qubit to another qubit, an important protocol for the transfer of quantum information[10,45]. In this algorithm, Alice wants to send a qubit state (which, in general, is unknown) to Bob. To do this, a Bell pair is generated, and one qubit from this pair is given to the sender, Alice, and the other qubit to the receiver, Bob. When the unknown state is ready to be teleported, it is entangled with Alice's qubit of the Bell pair. A subsequent measurement of both qubits by Alice yields two bits of classical information that she sends to Bob. With this information, Bob knows which of four possible rotations to apply to his qubit to obtain Alice's original unknown state.

Deterministic quantum teleportation has been demonstrated by the NIST[46] and Innsbruck[47] groups. The Innsbruck group used individual laser-beam addressing of three qubits; therefore, the state was teleported from one end of the ion string to the other end, a distance of ~10 μm. The NIST group used a multizone linear-trap array. By applying control potentials to electrode segments, the ions could be separated and moved in and out of one zone in which the laser beams were present. In this case, the state was teleported across a few hundred micrometres.

Teleportation is an important building block for quantum information processing and can reduce the computational resource requirements. Furthermore, it is the basic procedure for quantum communication protocols, such as for implementing quantum repeaters. Other algorithms — such as entanglement purification[48], quantum error correction[49], the quantum Fourier transform[50] and deterministic entanglement swapping (M. Riebe, T. Monz, K. Kim, A. S. Villar, P. Schindler, M. Chwalla, M. Hennrich and R. Blatt, unpublished observations) — have also been demonstrated with ion qubits.

These experiments demonstrate the basic features of quantum algorithms, but for the concatenation of processes and repeated computations, improved operation fidelities will be required. In particular, full and repetitive implementation of quantum error correction, which could keep a qubit superposition 'alive' while subjected to decoherence, remains a major challenge in quantum information processing.

## Applications

In the mid-1990s, a wave of interest in potential applications for quantum information processing was generated by Shor's period-finding algorithm for factoring large numbers[7]. Another noteworthy potential application is the implementation of unstructured searches[51]. However, to be of practical use, these applications require substantial resources in terms of the number of qubits and the number of operations, far beyond the capabilities of current implementations. Despite this, some elements of quantum information processing and entanglement with small numbers of qubits are beginning to find applications in metrology. Many physicists also expect that useful quantum simulations will be carried out on a relatively small number of qubits, perhaps up to 100, in the next decade.

One application in metrology is to improve interferometry. As an example, we discuss how entanglement can be applied to Ramsey spectroscopy[52], but this scheme has a direct analogue in electron, atom and photon Mach–Zehnder interferometry. Ramsey spectroscopy on the $|g\rangle \rightarrow |e\rangle$ transition proceeds as follows. The atom is first prepared in the state $|\Psi_{\text{initial}}\rangle = |g\rangle$. Radiation at frequency $\omega$ near $\omega_{eg}$ is applied in a fast pulse to produce the state $R_0(\pi/2, -\pi/2)|g\rangle = \frac{1}{\sqrt{2}}(|g\rangle + |e\rangle)$. The atom is now allowed to evolve for a duration $T$ so that the atom's upper state accumulates a phase $\phi_R = (\omega - \omega_{ge})T$ relative to the lower state (when the problem is viewed in a frame that rotates at frequency $\omega$). Finally, again, a rotation $R_0(\pi/2, -\pi/2)$ is applied and leaves the atom in the state (up to a global phase factor) $|\Psi_{\text{final}}\rangle = \sin(\phi_R/2)|g\rangle + i\cos(\phi_R/2)|e\rangle$. Therefore, the probability of finding the atom in the state $|e\rangle$ is $p_e = \frac{1}{2}(1 + \cos[(\omega - \omega_{ge})T])$. For an ensemble of $N$ atoms, the detected signal will be $Np_e$. In precision spectroscopy, the idea is to detect changes in $\omega - \omega_{ge}$ or $\phi_R$, as observed through changes in $p_e$. Therefore, the $N$-ion signal can be defined as $S = \mathrm{d}(Np_e)/\mathrm{d}\phi_R = -N/2\sin(\phi_R)$. The fundamental noise in the signal is given by the 'projection noise': that is, the fluctuation in the number of atoms, from experiment to experiment, that is measured to be in the state $|e\rangle$ (ref. 53). The variance of this noise is given by $V_N = Np_e(1 - p_e)$, so the magnitude of the signal-to-noise ratio is equal to $S/\sqrt{V_N} = \sqrt{N}$, essentially the shot noise corresponding to the number of atoms.

Now, suppose that the first $R_0(\pi/2, -\pi/2)$ pulse can be replaced with an entangling $\pi/2$ pulse[37,38], which creates the cat state

$$|g\rangle_1|g\rangle_2 \ldots |g\rangle_N \rightarrow \tfrac{1}{\sqrt{2}}(|g\rangle_1|g\rangle_2 \ldots |g\rangle_N + |e\rangle_1|e\rangle_2 \ldots |e\rangle_N) \equiv \tfrac{1}{\sqrt{2}}(|g_N\rangle + |e_N\rangle) \qquad (3)$$

After a delay $T$, the $|e_N\rangle$ state accumulates a phase $N\phi_R$ relative to the $|g_N\rangle$ state. A final entangling $\pi/2$ pulse leaves the atoms in a superposition state $\sin(N\phi_R/2)|g_N\rangle + i\cos(N\phi_R/2)|e_N\rangle$; therefore, the probability of detecting the atoms in the $|e_N\rangle$ state is $p_{N_e} = \frac{1}{2}(1 + \cos[N(\omega - \omega_{ge})T])$. It is as though spectroscopy has been carried out on a single 'super-atom' composed of states $|e_N\rangle$ and $|g_N\rangle$. The super-atom has a resonant frequency that is $N$ times higher than that of a single atom, as well as a phase sensitivity (to the $N$th harmonic of the applied radiation) that is $N$ times higher. The resultant gain in interferometric sensitivity must, however, be offset by the fact that only a single-particle two-state system ($|e_N\rangle$ and $|g_N\rangle$) is being measured. Nevertheless, after a statistically significant number of repeated measurements, the sensitivity is

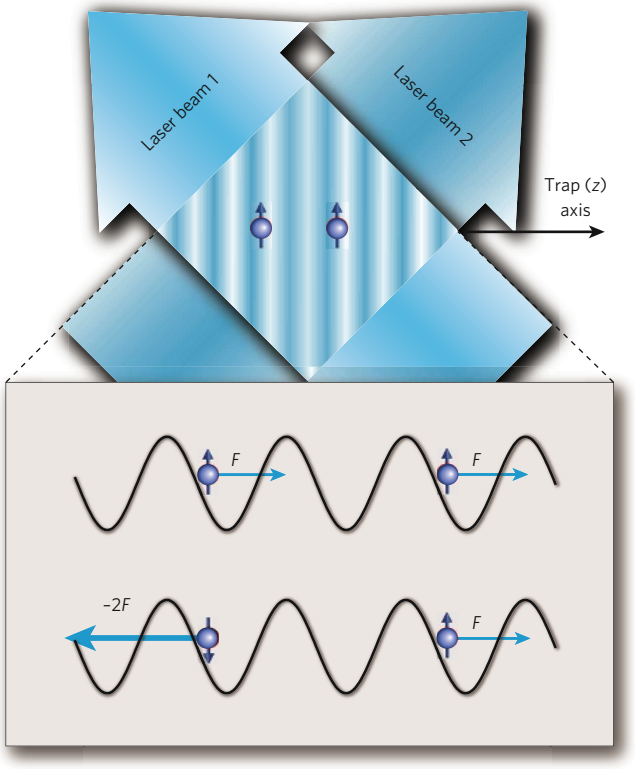


**Figure 3 | A two-qubit phase gate.** A phase gate with two ions (blue) is depicted. The operation of such phase gates relies on the fact that when a selected mode of the ions' motion is displaced in phase space about a closed path, the ions' wavefunction picks up a phase that is proportional to the enclosed area. If this displacement depends on the ions' qubit states, then entanglement is generated[92–95]. This state-dependent displacement can be implemented by applying optical dipole forces ($F$) by using laser-beam intensity gradients. In this example, an intensity standing wave is created with two laser beams, and the horizontal spacing of the ions is made to be an integral number of wavelengths of the intensity pattern. The pattern sweeps across the ions at the difference between the frequencies of the beams, chosen to be near the stretch-mode frequency. If the ions' qubit states $|g\rangle$ and $|e\rangle$ feel different dipole forces, then only the $|ge\rangle$ and $|eg\rangle$ components of the ions' wavefunction are displaced in phase space. By making the trajectories closed and by choosing the size of the displacements appropriately, the wavefunction is unchanged except for an $e^{i\pi/2}$ phase shift on the $|ge\rangle$ and $|eg\rangle$ states, the desired phase gate. Such gate operations have been implemented with trapped $^9Be^+$ ions[29,95] and in a similar way with $^{111}Cd^+$ ions[96] and $^{40}Ca^+$ ions[63,97].

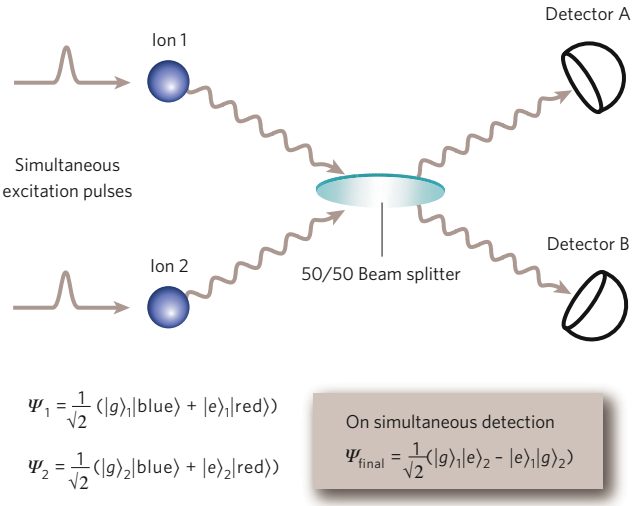


**Figure 4 | Entanglement produced by conditional measurements.** Entanglement can be created between two separated particles by an interference effect and state projection accompanying a measurement. In this example[25], it is assumed that the qubits of two ions (blue) are encoded in hyperfine levels of the electronic ground states. These qubits are first prepared in superposition states $\frac{1}{\sqrt{2}}(|g\rangle + |e\rangle)$. When excited with laser pulses that are short enough that both qubits simultaneously undergo (single-photon) scattering, the frequencies (denoted 'red' and 'blue') of the emitted photons along a particular direction are correlated with the qubit states, as indicated for entangled states $|\Psi_1\rangle$ and $|\Psi_2\rangle$. These photons can be simultaneously sent into a 50/50 beam splitter and then detected. In the cases when photons are simultaneously detected at detector A and detector B, the ions are projected into the Bell state $|\Psi_{\text{final}}\rangle$, even though the atoms have not directly interacted. For many such experiments, photons do not reach either detector; however, when photons are simultaneously detected, this 'heralds' the formation of the entangled state $|\Psi_{\text{final}}\rangle$, which can then be saved and used later, such as in Bell's inequality measurements of remotely located ions[98]. One potential use of this scheme is for entanglement-assisted communication between ion locations 1 and 2.

increased by a factor of $\sqrt{N}$ by using entangling $\pi/2$ pulses compared with the case of $N$ unentangled atoms[36–38]. Because of technical noise in the experiments, this theoretical improvement is not fully realized; however, a gain in sensitivity compared with the case of unentangled atoms has been realized for up to six entangled ions[38,54,55].

These arguments assume that noise results only from state projection. In experiments, if there is correlated decoherence of qubit phases, then any gain in sensitivity may be lost as a result of the faster decoherence of the cat states[56] or as a result of noise in the oscillator that produces the radiation[18,57]. If these sources of noise can be suppressed, entangled states should be able to improve the signal-to-noise ratio in future spectroscopy experiments.

Another application of quantum-information-processing techniques is increased fidelity of detection[58]. This can be useful if the qubit does not have a cycling transition or if the QND aspect of the shelving detection is not well satisfied. A simple implementation is to assume that there are two qubits, labelled q and d, stored in the same trap. The goal is to detect the state of information qubit q, by using detection qubit d. Before any measurements are taken, qubit q will generally be in a superposition state $\alpha|g\rangle_q + \beta|e\rangle_q$. Using the SWAP operations of the Cirac–Zoller gate, this superposition is first transferred to the qubit composed of the $|0\rangle$ and $|1\rangle$ states of a selected motional mode, and is then mapped to qubit d. Then, qubit d is measured, thereby in effect measuring qubit q. This protocol can be carried out without disturbing the initial probabilities $|\alpha|^2$ and $|\beta|^2$ for qubit q, even if the mapping steps are imperfect. Therefore, it is a QND measurement and can be repeated to increase detection efficiency. This scheme was demonstrated in an experiment[59] in which qubit q was based on an optical transition in a $^{27}Al^+$ ion and qubit d was based on a hyperfine transition in a $^9Be^+$ ion. In that experiment, a single round of detection had a fidelity of only $F = 0.85$; however, by repeating the measurement, and by using real-time bayesian analysis, the fidelity was improved to $F = 0.9994$. It should be noted that this strategy can also be used to prepare an eigenstate of qubit q with high fidelity. In addition to this demonstration, this protocol is now used in a high-accuracy optical clock based on single $^{27}Al^+$ ions[60]. This technique has also been extended so that a single detection qubit can be used to measure the states of multiple ions[59], similar to the measurement of the Fock states of photons by using multiple probe atoms[61].

Finally, entanglement can be used in metrology to create states that allow the measurement of certain parameters while suppressing sensitivity to others. This strategy has been used, for example, to make a precise measurement of the quadrupole moment of a $^{40}Ca^+$ ion by carrying out spectroscopy on an entangled state of two ions that depended on the quadrupole moment but was insensitive to fluctuations in the magnetic field[62].

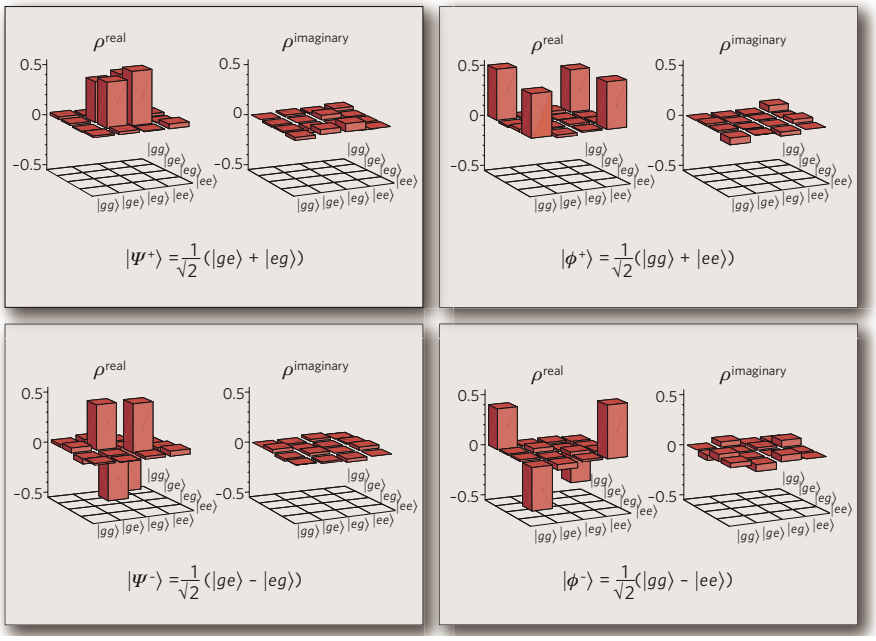


**Figure 5 | Measured density matrices of Bell states.** The real (left) and imaginary (right) parts of the density matrices obtained for the Bell states $|\Psi^+\rangle$ (upper left), $|\Psi^-\rangle$ (lower left), $|\phi^+\rangle$ (upper right) and $|\phi^-\rangle$ (lower right) prepared deterministically with two trapped $^{40}Ca^+$ ions are shown. The states were analysed by using quantum-state tomography, a technique that provides all of the necessary information to reconstruct the corresponding density matrix[8]. More specifically, the density matrix for a single qubit can be represented by $\rho = \frac{1}{2}(I + \Sigma_i \langle\sigma_i\rangle \sigma_i)$, where $\sigma_i$ is a Pauli matrix, $i = x, y, z$ and $I$ is the identity matrix. Measurements project a qubit onto its energy eigenstates, which is equivalent to measuring $\langle\sigma_z\rangle$. To determine $\langle\sigma_{x,y}\rangle$, an additional rotation of the Bloch sphere is applied before the measurement. The tomography procedure can be extended to $N$ qubits, requiring of the order of $4^N$ expectation values to be measured. Owing to statistical errors, the experimentally measured expectation values can result in unphysical elements in the density matrix (with negative eigenvalues). This outcome is avoided by fitting the measured expectation values by using a maximum-likelihood method and then finding the most likely density matrix that describes the state[28].

## Prospects

Although the basic elements of quantum computation have been demonstrated with atomic ions, operation errors must be significantly reduced and the number of ion qubits must be substantially increased if quantum computation is to be practical. Nevertheless, before fidelities and qubit numbers reach those required for a useful factoring machine, worthwhile quantum simulations might be realized.

### More ion qubits and better fidelity

To create many-ion entangled states, there are two important goals: improving gate fidelity, and overcoming the additional problems that are associated with large numbers of ions. For fault-tolerant operation, a reasonable guideline is to assume that the probability of an error occurring during a single gate operation should be of the order of $10^{-4}$ or lower. An important benchmark is the fidelity of two-qubit gates. The best error probability achieved so far is approximately $10^{-2}$, which was inferred from the fidelity of Bell-state generation[63]. In general, it seems that gate fidelities are compromised by limited control of classical components (such as fluctuations in the laser-beam intensity at the positions of the ions) and by quantum limitations (such as decoherence caused by spontaneous emission)[64]. These are daunting technical problems; however, eventually, with sufficient care and engineering expertise, these factors are likely to be suppressed.

The multiqubit operations discussed in this review rely on the ability to isolate spectrally a single mode of the motion of an ion. Because there are $3N$ modes of motion for $N$ trapped ions, as $N$ becomes large, the mode spectrum becomes so dense that the gate speeds must be significantly reduced to avoid off-resonance coupling to other modes. Several proposals have been put forward to circumvent this problem[65,66]. Alternatively, a way to solve this problem with gates that have been demonstrated involves distributing the ions in an array of multiple trap zones[18,67–69] (Fig. 6a). In this architecture, multiqubit gate operations could be carried out on a relatively small number of ions in multiple processing zones. Entanglement could be distributed between these zones by physically moving the ions[18,68,69] or by optical means[25,67,70–72]. For quantum communication over large distances, optical distribution seems to be the only practical choice; for experiments in which local entanglement is desirable, moving ions is also an option.

Examples of traps that could be used for scaling up the number of ions used in an algorithm are shown in Fig. 6b. Ions can be moved between zones by applying appropriate control electric potentials to the various electrode segments[46,73–75]. Individual ions have been moved ~1 mm in ~50 μs without loss of coherence; the excitation of the ion's motion (in its local well) was less than one quantum[73]. Multiple ions present in a single zone can be separated[46,73] by inserting an electric potential 'wedge' between the ions. In the teleportation experiment by the NIST group[46], two ions could be separated from a third in ~200 μs, with negligible excitation of the motional mode used for subsequent entangling operations between the two ions. This absence of motional excitation meant that an additional entangling-gate operation on the separated ions could be implemented with reasonable fidelity. For algorithms that operate over long time periods, the ions' motion will eventually become excited as a result of transportation and background noise from electric fields. To counteract this problem, additional laser-cooled ions could be used to cool the qubits 'sympathetically' (Fig. 6a). These 'refrigerator' ions could be identical to the qubit ions[76], of a different isotope[77] or of a different species[60,78]. They could also aid in detection and state preparation (described earlier).

For all multiqubit gates that have been implemented so far, the speeds are proportional to the frequencies of the modes of the ions, which scale as $1/d_{qe}^2$, where $d_{qe}$ is the distance of the ion to the nearest electrode. Therefore, it would be valuable to make traps as small as possible. Many groups have endeavoured to achieve this, but they have all observed significant heating of the ions, compromising gate fidelity. The heating is anomalously large compared with that expected to result from thermal noise, which arises from resistance in, or coupled to, the trap electrodes[18,79–83]. It scales approximately as $1/d_{qe}^4$ (refs 18, 79–83), which is consistent with the presence of independently fluctuating potentials on electrode patches, the extent of which is small compared with $d_{qe}$ (ref. 79). The source of the heating has yet to be understood, but recent experiments[80,82] indicate that it is thermally activated and can be significantly suppressed by operating at low temperature.

For large trap arrays, a robust means of fabrication will be required, as well as means of independently controlling a very large number of electrodes. Microelectromechanical systems (MEMS) fabrication technologies can be used for monolithic construction[83,84], and trap structures can be further simplified by placing all electrodes in a plane[84,85]. To mitigate the problem of controlling many electrodes, it might be possible to incorporate 'on-board' electronics close to individual trap zones[86]. Laser beams must also be applied in several locations simultaneously, because it will be essential to carry out parallel operations when implementing complex algorithms. The recycling of laser beams can be used[86,87], but the overall laser power requirements will still increase. If gates are implemented by using stimulated-Raman transitions, then a

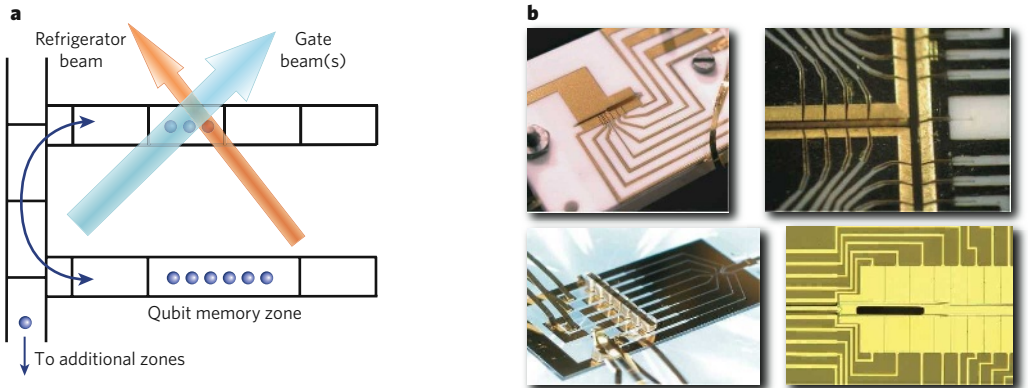


**Figure 6 | Multizone trap arrays. a**, A schematic representation of a multizone trap array is shown. Each control electrode is depicted as a rectangle. Ions (blue circles) can be separated and moved to specific zones, including a memory zone, by applying appropriate electrical potentials. Because the ions' motion will become excited as a result of transport (bidirectional arrow) and noisy ambient electric fields, refrigerator ions (red; which are cooled by the red laser beam) are used to cool the ions before gate operations, which are implemented with the blue laser beam. **b**, Examples of the electrode configurations of trap arrays are shown. In the upper left is a two-layer, six-zone linear trap in which entangled ions can be separated and used for algorithm demonstrations, including teleportation[46] (width of narrow slot (where the ions are located) = 200 μm). In the upper right is a three-layer, two-dimensional multizone trap that can be used to switch ion positions[99] (width of slot = 200 μm). In the lower left is a single-zone trap in which all of the electrodes lie in a single layer; this design considerably simplifies fabrication[85]. In the lower right is a single-layer, linear multizone trap fabricated on silicon (width of open slot for loading ions ≃ 95 μm), which can enable electronics to be fabricated on the same substrate that contains the trap electrodes. (Image courtesy of R. Slusher, Georgia Tech Research Institute, Atlanta).

high laser-beam intensity will also be needed to suppress spontaneous emission decoherence to fault-tolerant levels[64]. Detection will also need to be implemented simultaneously in several locations. This issue might be resolved by coupling on-board detectors or other forms of miniature integrated optics to optical fibres.

### Future applications

In the early 1980s, Feynman suggested that one quantum system could perhaps be used to simulate another[5]. This simulation could be accomplished efficiently with a large-scale quantum computer. But before this goal is reached, it might be possible to take advantage of the fact that current logic gates are implemented by hamiltonians that can be used to simulate interactions in other systems. A simple example was mentioned earlier in the discussion of spectroscopy with cat states; these experiments simulate the action of electron, photon and atom Mach–Zehnder interferometers that incorporate entangling beam splitters[55]. A more interesting prospect is that the gate hamiltonians might be applied in a strategic way to simulate specific many-body hamiltonians. The basic idea can be considered by noting that the two-ion phase gate (Fig. 3) can be written in the form $R_{Z1}R_{Z2}e^{-i\xi\sigma_{z1}\sigma_{z2}}$, where $R_{Z1}$ and $R_{Z2}$ are rotations about the $z$ axis and $\xi$ is the strength of coupling. Therefore, up to an overall rotation on the qubits, the gate implements the hamiltonian $H=\hbar\kappa\sigma_{z1}\sigma_{z2}$, a spin–spin interaction between the two addressed spins, where $\kappa$ is the strength of the interaction and $\hbar$ is $h/2\pi$ (and $h$ is Planck's constant). By extending these couplings to many ion qubits in an ensemble, Ising-type spin hamiltonians could, for example, be implemented[88–91]. The interactions between ion pairs could be applied in a stepwise manner but might also be implemented simultaneously, thereby increasing efficiency. Although simulating specific many-body hamiltonians is a challenge given current experimental capabilities, even with a relatively small number of ions, interesting phenomena such as quantum phase transitions might be observable.

## Conclusion

As researchers progress towards generating a large-scale quantum-information-processing device, it might be possible to shed light on more fundamental issues of decoherence and why many-particle states with the quantum attributes of Schrödinger's cat are not observed. If it is possible to continue scaling up such devices to a large size, the issue of the absence of cat states becomes more pressing. For example, suppose that, in the future, large-$N$-qubit cat states in the form of equation (3) can be made. Then, this cat state for $N$ qubits can be rewritten as $|\Psi\rangle=\frac{1}{\sqrt{2}}(|g\rangle_j\pi_{k\neq j}^N|g\rangle_k+|e\rangle_j\pi_{k\neq j}^N|e\rangle_k)$, where the $j$th qubit has been (arbitrarily) singled out and $k$ represents the other qubits. For large $N$, this wavefunction has the attributes of Schrödinger's cat in the sense that the states of a single two-level quantum system (the $j$th qubit) are correlated with states that have macroscopically distinct polarizations. If generating such states is successful, then the existence of, in essence, Schrödinger's cats will have been shown. Such states are, however, more sensitive to the effects of phase decoherence[56], but this seems to be a technical, not a fundamental, problem. Therefore, if it becomes impossible to make such states or to build a large-scale quantum computer for non-technical reasons, this failure might indicate some new physics. ■


1. Ramsey, N. F. *Molecular Beams* (Clarendon, London, 1956).
2. Freedman, S. F. & Clauser, J. F. Experimental test of local hidden-variable theories. *Phys. Rev. Lett.* **28,** 938–941 (1972).
3. Aspect, A., Grangier, P. & Roger, G. Experimental tests of realistic local theories via Bell's theorem. *Phys. Rev. Lett.* **47,** 460–463 (1981).
4. Bell, J. S. *Speakable and Unspeakable in Quantum Mechanics* (Cambridge Univ. Press, Cambridge, UK, 1987).
5. Feynman, R. P. Simulating physics with computers. *Int. J. Theoret. Phys.* **21,** 467–468 (1982).
6. Deutsch, D. Quantum theory, the Church–Turing principle and the universal quantum computer. *Proc. R. Soc. Lond. A* **400,** 97–117 (1985).
7. Shor, P. W. Algorithms for quantum computation: discrete logarithms and factoring. In *Proc. Annu. Symp. Found. Comput. Sci.* 124–134 (1994).
8. Nielsen, M. A. & Chuang, I. L. *Quantum Computation and Quantum Information* (Cambridge Univ. Press, Cambridge, UK, 2000).
9. Cirac, J. I. & Zoller, P. Quantum computations with cold trapped ions. *Phys. Rev. Lett.* **74,** 4091–4094 (1995).
10. Monroe, C. Quantum information processing with atoms and photons. *Nature* **416,** 238–246 (2002).
11. Dehmelt, H. Experiments with an isolated subatomic particle at rest. *Rev. Mod. Phys.* **62,** 525–530 (1990).
12. Paul, W. Electromagnetic traps for charged and neutral particles. *Rev. Mod. Phys.* **62,** 531–540 (1990).
13. Bollinger, J. J., Heinzen, D. J., Itano, W. M., Gilbert, S. L. & Wineland, D. J. A 303-MHz frequency standard based on trapped $^9Be^+$ ions. *IEEE Trans. Instrum. Meas.* **40,** 126–128 (1991).
14. Fisk, P. T. H. *et al.* Very high q microwave spectroscopy on trapped $^{171}Yb^+$ ions: application as a frequencystandard. *IEEE Trans. Instrum. Meas.* **44,** 113–116 (1995).
15. Blatt, R., Häffner, H., Roos, C., Becher, C. & Schmidt-Kaler, F. in *Quantum Entanglement and Information Processing: Les Houches Session LXXIX* (eds Estève, D. Raimond, J.-M. & Dalibard, J.) 223–260 (Elsevier, Amsterdam, 2004).
16. Wineland, D. J. in *Quantum Entanglement and Information Processing: Les Houches Session LXXIX* (eds Estève, D. Raimond, J.-M. & Dalibard, J.) 261–293 (Elsevier, Amsterdam, 2004).
17. Leibfried, D., Blatt, R., Monroe, C. & Wineland, D. Quantum dynamics of single trapped ions. *Rev. Mod. Phys.* **75,** 281–324 (2003).
18. Wineland, D. J. *et al.* Experimental issues in coherent quantum-state manipulation of trapped atomic ions. *J. Res. Natl Inst. Stand. Technol.* **103,** 259–328 (1998).
19. Diedrich, F., Bergquist, J. C., Itano, W. M. & Wineland, D. J. Laser cooling to the zero-point energy of motion. *Phys. Rev. Lett.* **62,** 403–406 (1989).
20. Dehmelt, H. G. Mono-ion oscillator as potential ultimate laser frequency standard. *IEEE Trans. Instrum. Meas.* **31,** 83–87 (1982).
21. Monroe, C., Meekhof, D. M., King, B. E., Itano, W. M. & Wineland, D. J. Demonstration of a fundamental quantum logic gate. *Phys. Rev. Lett.* **75,** 4714–4717 (1995).
22. Schmidt-Kaler, F. *et al.* Realization of the Cirac–Zoller controlled-NOT quantum gate. *Nature* **422,** 408–411 (2003).
23. Schmidt-Kaler, F. *et al.* How to realize a universal quantum gate with trapped ions. *Appl. Phys. B* **77,** 789–796 (2003).
24. Riebe, M. *et al.* Process tomography of ion trap quantum gates. *Phys. Rev. Lett.* **97,** 220407 (2006).
25. Moehring, D. L. *et al.* Entanglement of single-atom quantum bits at a distance. *Nature* **449,** 68–71 (2007).
26. Turchette, Q. A. *et al.* Deterministic entanglement of two trapped ions. *Phys. Rev. Lett.* **81,** 3631–3634 (1998).
27. Rowe, M. A. *et al.* Experimental violation of a Bell's inequality with efficient detection. *Nature* **409,** 791–794 (2001).
28. Roos, C. F. *et al.* Bell states of atoms with ultralong life times and their tomographic state analysis. *Phys. Rev. Lett.* **92,** 220402 (2004).
29. Sackett, C. A. *et al.* Experimental entanglement of four particles. *Nature* **404,** 256–259 (2000).
30. Clauser, J. F., Horne, M. A., Shimony, A. & Holt, R. A. Proposed experiment to test local hidden-variable theories. *Phys. Rev. Lett.* **23,** 880–884 (1969).
31. Moehring, D. L., Madsen, M. J., Blinov, B. B. & Monroe, C. Experimental Bell inequality violation with an atom and a photon. *Phys. Rev. Lett.* **93,** 090410 (2004).
32. Schrödinger, E. Die gegenwärtige Situation in der Quantenmechanik. *Naturwissenschaften* **23,** 807–812 (1935).
33. Greenberger, D. M., Horne, M. A. & Zeilinger, A. in *Going Beyond Bell's Theorem* (ed. Kafatos, M.) 69–72 (Kluwer Academic, Dordrecht, 1989).
34. DiVincenzo, D. P. & Shor, P. W. Fault-tolerant error correction withefficient quantum codes. *Phys. Rev. Lett.* **77,** 3260–3263 (1996).
35. Steane, A. M. Error correcting codes in quantum theory. *Phys. Rev. Lett.* **77,** 793–797 (1996).
36. Bollinger, J. J., Itano, W. M., Wineland, D. J. & Heinzen, D. J. Optimal frequency measurements with maximally correlated states. *Phys. Rev. A* **54,** R4649–R4652 (1996).
37. Leibfried, D. *et al.* Toward Heisenberg-limited spectroscopy with multiparticle entangled states. *Science* **304,** 1476–1478 (2004).
38. Leibfried, D. *et al.* Creation of a six-atom 'Schrödinger cat' state. *Nature* **438,** 639–642 (2005).
39. Roos, C. F. *et al.* Control and measurement of three-qubit entangled states. *Science* **304,** 1478–1480 (2004).
40. Dür, W., Vidal, G. & Cirac, J. I. Three qubits can be entangled in two inequivalent ways. *Phys. Rev. A* **62,** 062314 (2000).
41. Häffner, H. *et al.* Scalable multiparticle entanglement of trapped ions. *Nature* **438,** 643–646 (2005).
42. Deutsch, D. & Jozsa, R. Rapid solution of problems by quantum computation. *Proc. R. Soc. Lond. A* **439,** 553–558 (1992).
43. Chuang, I. L. *et al.* Experimental realization of a quantum algorithm. *Nature* **393,** 143–146 (1998).
44. Gulde, S. *et al.* Implementation of the Deutsch–Jozsa algorithm on an ion-trap quantum computer. *Nature* **421,** 48–50 (2003).
45. Bennett, C. H. *et al.* Teleporting an unknown quantum state via dual classical and Einstein–Podolsky-Rosen channels. *Phys. Rev. Lett.* **70,** 1895–1899 (1993).
46. Barrett, M. D. *et al.* Deterministic quantum teleportation of atomic qubits. *Nature* **429,** 737–739 (2004).
47. Riebe, M. *et al.* Deterministic quantum teleportation with atoms. *Nature* **429,** 734–737 (2004).
48. Reichle, R. *et al.* Experimental purification of two-atom entanglement. *Nature* **443,** 838–841 (2006).
49. Chiaverini, J. *et al.* Realization of quantum error correction. *Nature* **432,** 602–605 (2004).
50. Chiaverini, J. *et al.* Implementation of the semiclassical quantum Fourier transform in a scalable system. *Science* **308,** 997–1000 (2005).
51. Grover, L. K. Quantum mechanics helps in searching for a needle in a haystack. *Phys. Rev. Lett.* **79,** 325–328 (1997).
52. Wineland, D. J., Bollinger, J. J., Itano, W. M., Moore, F. L. & Heinzen, D. J. Spin squeezing and reduced quantum noise in spectroscopy. *Phys. Rev. A* **46,** R6797–R6800 (1992).

53. Itano, W. M. *et al.* Quantum projection noise: population fluctuations in two-level systems. *Phys. Rev. A* **47,** 3554–3570 (1993).
54. Meyer, V. *et al.* Experimental demonstration of entanglement-enhanced rotation angle estimation using trapped ions. *Phys. Rev. Lett.* **86,** 5870–5873 (2001).
55. Leibfried, D. *et al.* Trapped-ion quantum simulator: experimental application to nonlinear interferometers. *Phys. Rev. Lett.* **89,** 247901 (2002).
56. Huelga, S. F. *et al.* Improvement of frequency standards with quantum entanglement. *Phys. Rev. Lett.* **79,** 3865–3868 (1997).
57. André, A., Sørensen, A. S. & Lukin, M. D. Stability of atomic clocks based on entangled atoms. *Phys. Rev. Lett.* **92,** 230801 (2004).
58. Schaetz, T. *et al.* Enhanced quantum state detection efficiency through quantum information processing. *Phys. Rev. Lett.* **94,** 010501 (2005).
59. Hume, D. B., Rosenband, T. & Wineland, D. J. High-fidelity adaptive qubit detection through repetitive quantum nondemolition measurements. *Phys. Rev. Lett.* **99,** 120502 (2007).
60. Rosenband, T. *et al.* Frequency ratio of $Al^+$ and $Hg^+$ single-ion optical clocks; metrology at the 17th decimal place. *Science* **319,** 1808–1812 (2008).
61. Guerlin, C. *et al.* Progressive field-state collapse and quantum non-demolition photon counting. *Nature* **448,** 889–894 (2007).
62. Roos, C. F., Chwalla, M., Kim, K., Riebe, M. & Blatt, R. 'Designer atoms' for quantum metrology. *Nature* **443,** 316–319 (2006).
63. Benhelm, J., Kirchmair, G., Roos, C. F. & Blatt, R. Towards fault-tolerant quantum computing with trapped ions. *Nature Phys.* **4,** 463–466 (2008).
64. Ozeri, R. *et al.* Errors in trapped-ion quantumgates due to spontaneous photon scattering. *Phys. Rev. A* **75,** 042329 (2007).
65. Zhu, S.-L., Monroe, C. & Duan, L.-M. Arbitrary-speed quantum gates within large ion crystals through miminum control of laser beams. *Europhys. Lett.* **73,** 485–491 (2006).
66. Duan, L.-M. Scaling ion trap quantum computation through fast quantum gates. *Phys. Rev. Lett.* **93,** 100502 (2004).
67. DeVoe, R. G. Elliptical ion traps and trap arrays for quantum computation. *Phys. Rev. A* **58,** 910–914 (1998).
68. Cirac, J. I. & Zoller, P. A scalable quantum computer with ions in an array of microtraps. *Nature* **404,** 579–581 (2000).
69. Kielpinski, D., Monroe, C. & Wineland, D. J. Architecture for a large-scale ion-trap quantum computer. *Nature* **417,** 709–711 (2002).
70. Cirac, I., Zoller, P., Kimble, J. & Mabuchi, H. Quantum state transfer and entanglement distribution among distant nodes in a quantum network. *Phys. Rev. Lett.* **78,** 3221–3224 (1997).
71. Duan, L.-M. & Kimble, H. J. Scalable photonic quantum computation through cavity-assisted interactions. *Phys. Rev. Lett.* **92,** 127902 (2004).
72. Duan, L.-M. *et al.* Probabilistic quantum gates between remote atoms through interference of optical frequency qubits. *Phys. Rev. A* **73,** 062324 (2006).
73. Rowe, M. *et al.* Transport of quantum states and separation of ions in a dual rf ion trap. *Quantum Inform. Comput.* **2,** 257–271 (2002).
74. Hucul, D. *et al.* On the transport of atomic ions in linear and multidimensional trap arrays. Preprint at <http://arxiv.org/abs/quant-ph/0702175> (2007).
75. Huber, G. *et al.* Transport of ions in a segmented linear Paul trap in printed-circuit-board technology. *New J. Phys.* **10,** 013004 (2008).
76. Rohde, H. *et al.* Sympathetic ground-state cooling and coherent manipulation with two-ion crystals. *J. Opt. Soc. Am. B* **3,** S34–S41 (2001).
77. Blinov, B. B. *et al.* Sympathetic cooling of trapped $Cd^+$ isotopes. *Phys. Rev. A* **65,** 040304 (2002).
78. Barrett, M. D. *et al.* Sympathetic cooling of $^9Be^+$ and $^{24}Mg^+$ for quantum logic. *Phys. Rev. A* **68,** 042302 (2003).
79. Turchette, Q. A. *et al.* Heating of trapped ions from the quantum ground state. *Phys. Rev. A* **61,** 063418 (2000).
80. Deslauriers, L. *et al.* Scaling and suppression of anomalous heating in ion traps. *Phys. Rev. Lett.* **97,** 103007 (2006).
81. Leibrandt, D., Yurke, B. & Slusher, R. Modeling ion trap thermal noise decoherence. *Quant. Inform. Comput.* **7,** 52–72 (2007).
82. Labaziewicz, J. *et al.* Suppression of heating rates in cryogenic surface-electrode ion traps. *Phys. Rev. Lett.* **100,** 013001 (2008).
83. Stick, D. *et al.* Ion trap in a semiconductor chip. *Nature Phys.* **2,** 36–39 (2006).
84. Chiaverini, J. *et al.* Surface-electrode architecture for ion-trap quantum information processing. *Quantum Inform. Comput.* **5,** 419–439 (2005).
85. Seidelin, S. *et al.* Microfabricated surface-electrode ion trap for scalable quantum information processing. *Phys. Rev. Lett.* **96,** 253003 (2006).
86. Kim, J. *et al.* System design for large-scale ion trap quantum information processor. *Quant. Inform. Comput.* **5,** 515–537 (2005).
87. Leibfried, D., Knill, E., Ospelkaus, C. & Wineland, D. J. Transport quantum logic gates for trapped ions. *Phys. Rev. A* **76,** 032324 (2007).
88. Wunderlich, C. & Balzer, C. Quantum measurements and new concepts for experiments with trapped ions. *Adv. At. Mol. Opt. Phys.* **49,** 293–376 (2003).
89. Porras, D. & Cirac, J. I. Quantum manipulation of trapped ions in two dimensional Coulomb crystals. *Phys. Rev. Lett.* **96,** 250501 (2006).
90. Taylor, J. M. & Calarco, T. Wigner crystals of ions as quantum hard drives. Preprint at <http://arxiv.org/abs/0706.1951> (2007).
91. Chiaverini, J. & Lybarger Jr, W. E. Laserless trapped-ion quantum simulations without spontaneous scattering using microtrap arrays. *Phys. Rev. A* **77,** 022324 (2008).
92. Mølmer, K. & Sørensen, A. Multiparticle entanglement of hot trapped ions. *Phys. Rev. Lett.* **82,** 1835–1838 (1999).
93. Milburn, G. J., Schneider, S. & James, D. F. Ion trap quantum computing with warm ions. *Fortschr. Physik* **48,** 801–810 (2000).
94. Solano, E., de Matos Filho, R. L. & Zagury, N. Mesoscopic superpositions of vibronic collective states of *N* trapped ions. *Phys. Rev. Lett.* **87,** 060402 (2001).
95. Leibfried, D. *et al.* Experimental demonstration of a robust, high-fidelity geometric two ion-qubit phase gate. *Nature* **422,** 412–415 (2003).
96. Haljan, P. C. *et al.* Entanglement of trapped-ion clock states. *Phys. Rev. A* **72,** 062316 (2005).
97. Home, J. P. *et al.* Deterministic entanglement and tomography of ion spin qubits. *New J. Phys.* **8,** 188 (2006).
98. Matsukevich, D. N., Maunz, P., Moehring, D. L., Olmschenk, S. & Monroe, C. Bell inequality violation with two remote atomic qubits. *Phys. Rev. Lett.* **100,** 150404 (2008).
99. Hensinger, W. K. *et al.* T-junction ion trap array for two-dimensional ion shuttling storage, and manipulation. *Appl. Phys. Lett.* **88,** 034101 (2006).


**Acknowledgements** We thank H. Häffner, J. Home, E. Knill, D. Leibfried, C. Roos and P. Schmidt for comments on the manuscript.

**Author Information** Reprints and permissions information is available at www.nature.com/reprints. The authors declare no competing financial interests. Correspondence should be addressed to R.B. (Rainer.Blatt@uibk.ac.at).